Comput Mech (2010) 46:635–640
DOI 10.1007/s00466-010-0500-6

ORIGINAL PAPER

Long-range correlations of elastic fields in semi-flexible fiber networks

R. C. Picu · H. Hatami-Marbini

Received: 27 July 2009 / Accepted: 16 April 2010 / Published online: 1 June 2010

Abstract The mechanical properties of semi-flexible networks have been the subject of intense theoretical and experimental studies concerned primarily with the understanding of the complex behavior of biological systems such as the cell. Here it is shown that the elasticity of these networks, both elastic constants and elastic fields, while fluctuating significantly with position, is long-range correlated and the correlation functions exhibit power law scaling. The correlations are lost when the fiber stiffness is reduced. The range of scales over which correlations are observed is bounded below by the mean fiber segment length and above by the filament persistence length. Therefore, these networks can be regarded as stochastic fractal elastic media over the respective range of scales. This implies that no scale decoupling exists and no representative volume element can be identified on scales below the upper correlation cut-off scale.

Keywords Fractals · Homogenization · Stochastic · Elasticity · Microstructural

1 Introduction

Semi-flexible random fiber networks are the building blocks of many biological and non-biological systems. For example, the cytoskeleton of eukaryotic cells is composed from a set of interpenetrating semi-flexible fiber networks, with the F-actin and the microtubules networks being the main constituents. This structure plays a complex role in the mechanics of the cell, in the transport of biomolecules within the cytoplasm, in chemo-mechanical transduction and signaling e.g. [1,2]. The collagenous extra-cellular matrix and artificial tissue scaffolds are other examples of networks whose local elasticity determines to a large extent cellular growth rates.

The system-scale properties of semi-flexible networks are quite different from those of flexible fiber networks [3–5]. For example, in the case of the cytoskeleton, localized mechanical perturbations ("point forces") produce strain fields which are longer ranged than what would be expected from a continuum with homogeneous properties. When subjected to oscillatory loading, the dynamic response exhibits power law scaling over a broad range of frequencies [6].

The mechanics of fibrous networks was studied extensively analytically [7,8], experimentally [9–11] and by means of simulations [12–14]. Like many other disordered media [15–18], the deformation of these networks is non-affine [12,13,19–21]. It was observed that the non-affinity, defined as the fluctuation of the strain field, exhibits power law scaling with the scale of observation [22,23].

Here we show that this scaling is a consequence of the fact that, when probed on a local scale, the network exhibits elastic constants that fluctuate significantly with the position, but are long-range power law correlated. This leads to strains (and average stresses) having similar correlations. The scaling range is bounded above by the fiber length. At larger length scales, as well as in flexible fiber networks, correlations are lost and the networks can be homogenized using standard methods of mechanics. It is noted that the density of all systems considered here is larger than the percolation density (the density at which a continuously connected path spanning the entire problem domain can be

R. C. Picu
Department of Mechanical, Aerospace and Nuclear Engineering, Rensselaer Polytechnic Institute, Troy, NY 12180, USA

H. Hatami-Marbini (✉)
Mechanical Engineering Department, Stanford University, Stanford, CA 94305, USA
e-mail: hhatami@stanford.edu

found) and hence the effect discussed is not related to this threshold.

2 The model

Let us consider a two-dimensional network generated by depositing semi-flexible fibers of length L_0 in a square domain of dimension L. Fibers are placed randomly and their orientation distribution is uniform. They are connected to each other rigidly at the intersection points. Fibers are characterized by their bending and axial stiffness, κ and η respectively, while their excluded volume is not taken into account. The system is loaded by imposing displacements (a far-field strain) along the boundary of the domain and the solution is evaluated by minimizing the potential energy of the system.

Various "characteristic length scales" have been identified for such systems: the fiber length, L_0, the mean segment length, l_c (which is related to the fiber number density through the Corte–Kallmes theory [24], Fig. 1), and $l_b = \sqrt{\kappa/\eta}$ which represents the relative importance of bending, κ, and axial, η, stiffnesses. In the models discussed here, the system size is $L/L_0 = 20$, l_b/L_0 ranges from 0.0001 to 0.01, and the fiber number density, N, is varied from 200 to 800 fibers per unit area, which corresponds to mean segment lengths l_c/L_0 ranging from 0.009 to 0.031, Fig. 1.

In order to probe its elastic response, the network is loaded in uniform uniaxial tension (by imposing displacements along the boundary of the model) and the displacements at all network nodes (points where fibers cross) are evaluated by minimizing the potential energy, U_p, of the entire structure,

$$U_p = \sum_i \int \frac{1}{2}\kappa_i \left(\nabla^2 u_i(s)\right)^2 ds + \int \frac{1}{2}\eta_i \left(\frac{dl_i(s)}{ds}\right)^2 ds, \quad (1)$$

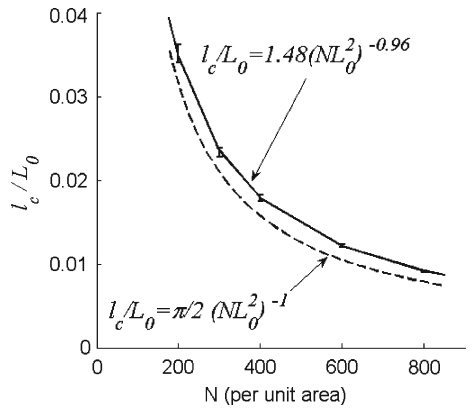

Fig. 1 Normalized mean fiber segment length l_c/L_0 as a function of fiber number density, N. The *continuous line* is the best fit to the numerical data, while the *dashed line* is the prediction of the Corte–Kallmes theory [24]

where u_i is the transverse displacement of fiber i, s is its contour length, $dl_i(s)/ds$ is the axial strain and κ_i, η_i are the bending and axial stiffnesses of fiber i. The sum is performed over all fibers. Since the boundary value problem is defined in terms of imposed displacements, the work done on the structure does not appear in the expression of U_p. The two functions $u_i(s)$ and $l_i(s)$ are written in terms of the displacements of the network nodes by using finite element interpolation functions.

The resulting elastic fields are probed by overlaying a virtual regular mesh of square elements of size $\delta/L_0 (\ll 1)$. This parameter defines the probing length scale. This is shown schematically in Fig. 2 where the network is represented in blue and the probing mesh in red. A mesh element, highlighted in black, is zoomed in to show its "microstructure." The density per element is computed based on the total length of fibers in the respective domain of area δ^2. In order to maintain the density above a critical value and to insure that measuring the mechanics of the respective patch is meaningful, δ is taken larger than $\delta_0 = l_c$.

The effective (average) stress and strain are evaluated for each square domain of the probing mesh. To this end, each square domain is considered separately and the points of intersection of fibers with its edges are determined. Their displacement is known from the solution of the global discrete problem. The axial force and bending moment acting at each of these intersection points can be evaluated from

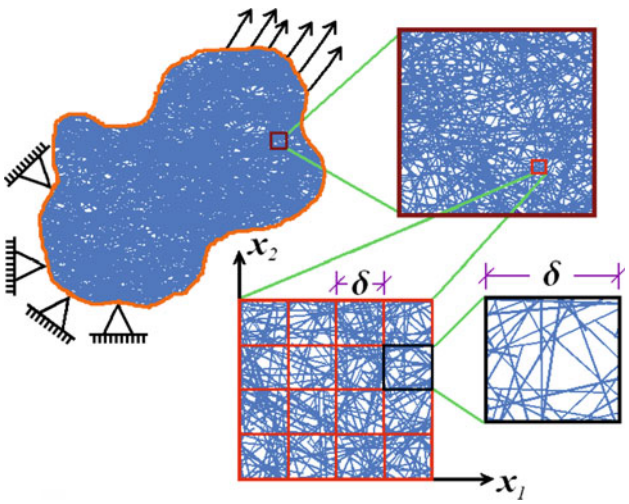

Fig. 2 Consider a dense fiber network composed from a large number of fibers of similar properties, subjected to specified boundary conditions (imposed tractions or displacements). The density and elasticity of the network are analyzed by dividing the domain using a regular mesh of characteristic dimension δ and computing the total fiber length (density) in each square sub-domain. Furthermore, the partition is used to determine the effective elastic moduli for each square sub-domain, as described in text. The mesh is used for probing and extends over the entire problem domain, but is shown here on an intermediate scale only for clarity

the network nodal displacements. This information is used to evaluate the displacement and traction distributions along the perimeter of each square domain of size δ. Linear interpolation functions are used to infer the average strain and stress state per element. The elastic constants in each element are then computed based on the local stress and strain. This fitting can be performed only if the fiber density in the respective element is sufficiently large; this condition led to the threshold $\delta_0 = l_c$ mentioned above. It must also be insured that the total bending moment obtained by summing up distributed moments along each element edge is negligible; if this condition is not fulfilled, a micro-polar formulation of elasticity must be used instead. The resulting stress field is an equilibrium field because the underlying network is in equilibrium. The resulting strain field is compatible both locally and globally because linear interpolation functions are used. Moreover, this fitting insures the compatibility of the deformation of neighboring elements (a situation similar to that in finite element models).

The results of this procedure were tested against an alternative method for finding the elastic constants in each element of size δ. This method is based on treating the overlay mesh as a finite element mesh and obtaining the solution to the specified far field boundary conditions subjected to the constraint that the strain energy in each element is equal to the strain energy of the underlying patch of fiber network, and to the global (least squares) condition that the displacements computed with this continuum model are closest possible to those evaluated with the discrete model. The unknown variables in this formulation are the mesh nodal displacements, $\mathbf{u}_k^{FE}$, and the elastic constants in each element. The displacement of network nodes at position $x^{(l)}$ can be written as

$$\mathbf{u}^{\mathrm{Cont}}\left(\mathbf{x}^{(l)}\right) = \sum_{k=1}^{N^{FE}} N_k\left(\mathbf{x}^{(l)}\right)\mathbf{u}_k^{FE}, \tag{2}$$

where $\mathbf{N}_k(\mathbf{x}^{(l)})$ is the interpolation function for node k of the FE mesh evaluated at the location of the l-th network node, and N^{FE} denotes the total number of mesh nodes in the FE model. In order to obtain the unknown FE nodal displacements, $\mathbf{u}_k^{FE}$, the norm of the difference between the actual displacements $\mathbf{u}(\mathbf{x}^{(l)})$ of the network nodes and their corresponding FE estimates $\mathbf{u}^{\mathrm{Cont}}(\mathbf{x}^{(l)})$ is minimized subjected to the constraint that the continuum elastic strain energy of each square element i, U_i^{Cont}, is equal to the corresponding discrete strain energy U_i. The discrete energy is the sum of the strain energy of all fibers in the domain of element l and the continuum elastic energy is given in terms of unknown elastic constants of the equivalent continuum element i. The two methods lead to similar local moduli and to identical Young's modulus ACFs [25].

3 Results

The auto-correlation function (ACF) of the density is computed from the continuum map of the fiber density and is shown in Fig. 3a for networks with various mean segment lengths probed at several length scales δ/l_c. The curves are normalized with the variance of the respective field. The ACF is evaluated by averaging over multiple origins and over all radial lines passing through the current origin. r represents the distance from the reference point. The function is a power law over the given range, with exponent independent of the fiber density (l_c/L_0) and of the probing length scale, δ, $\mathrm{ACF}_\rho(r) \sim r^{-s\rho}$. The exponent results approximately $s_\rho = 0.88 \pm 0.04$. This indicates a fractal box dimension for

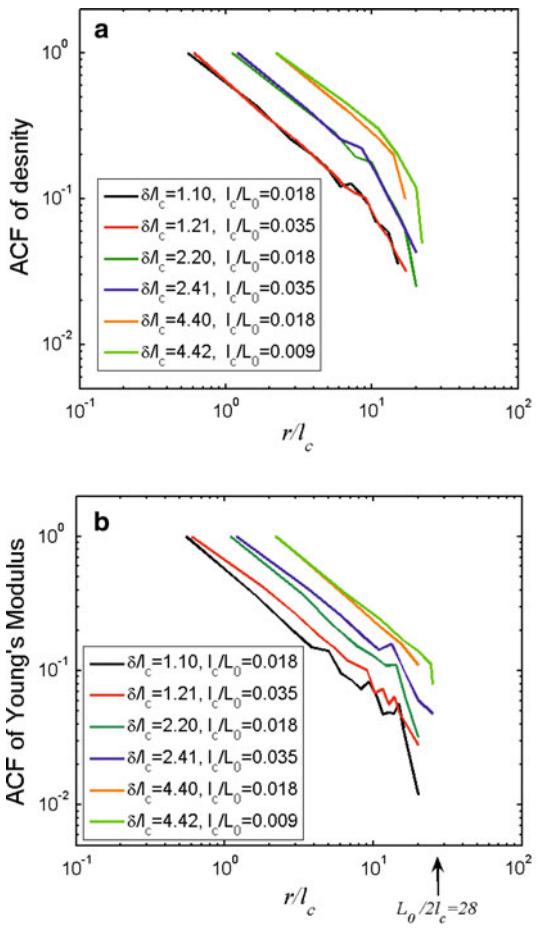

Fig. 3 Auto-correlation functions (ACF) of **a** fiber density and **b** effective Young's modulus E distribution for networks of various densities (mean segment lengths l_c/L_0) and of $l_b/L_0 = 0.01$, probed on various scales, δ/lc. Using the procedure described in text, a density and a set of moduli are assigned to each square sub-domain of size δ shown in Fig. 2. The ACF of both quantities is a power law for r smaller than approximately half of the fiber length, L_0. This upper cut-off is indicated in **b** for the network with $l_c/L_0 = 0.018$. The scaling exponent is independent of the fiber number density and of the probing length scale, δ

the density surface of $D_\rho = 3 - s_\rho/2 = 2.56 \pm 0.02$ [26]. The dimension is larger than 2, indicating a fractal rough surface. The range of power law scaling is bounded above by approximately $L_0/2$, threshold beyond which the ACF drops to zero.

The physical origin of this observation can be clarified by the following analysis. Let us consider that one drops N fibers of length $L_0 (L_0 \gg \delta)$ per unit area, such that the generic element i of size δ receives $\bar{n}_\delta + \Delta n_i$ fiber centers. $\bar{n}_\delta$ is the mean number of fiber centers (i.e. $\bar{n}_\delta = N\delta^2$) and Δn_i represents the variation from the mean of the number in element i. These fibers contribute to the total fiber density (fiber length by the element area) in element i by $\sim (\bar{n}_\delta + \Delta n_i)\delta/\delta^2$.

In addition to the fibers with center in element i, the element is also crossed by fibers with centers in element j located at a distance r_{ij} from $i, r_{ij} < L_0/2$. The probability of a fiber centered in element j to cross element i is approximately $p(r_{ij}) = \frac{1}{2\pi}\frac{\delta}{r_{ij}}$. Hence, the total number of fibers centered elsewhere and crossing element i is $\sum_{k=1}^{M_i} p(r_{ik})(\bar{n}_\delta + \Delta n_k)$ where M_i is the number of elements k for which $r_{ik} < L_0/2$. The total fiber density in element i results

$$\rho_i = \left[\bar{n}_\delta + \Delta n_i + \sum_{k=1}^{M_i} p(r_{ik})(\bar{n}_\delta + \Delta n_k)\right] \Big/ \delta. \tag{3}$$

It is now possible to compute the density auto-correlation function as $ACF_\rho(r_{ij}) = \langle(\rho_i - \langle\rho_i\rangle)(\rho_j - \langle\rho_j\rangle)\rangle$. Considering that the number of fibers with centers in i is not correlated with the respective number of fibers in any other element j, i.e. $\langle \Delta n_i \Delta n_j \rangle = \sigma_N^2 \delta_{ij}$ (δ_{ij} is the Kronecker delta function) and $\langle \Delta n_i \rangle = \langle \Delta n_j \rangle = 0$,

$$\mathrm{ACF}_\rho(r_{ij}) = \sigma_N^2 \left[\frac{1}{\pi r_{ij}\delta}\bigg|_{r_{ij}<\frac{L_0}{2}} + \frac{1}{4\pi^2}\sum_{k=1}^{M}\frac{1}{r_{ik}r_{jk}}\bigg|_{r_{ij}<L_0}\right]. \tag{4}$$

where σ_N^2 is the fluctuation of the number of fibers in an element produced by the Poisson process used to generate the network. The sum is performed over all elements k located in the intersection domain Q of two circles of radius $L_0/2$ centered at i and j. M denotes the number of squares of area δ^2 in domain Q, Fig. 4. The first term in (3) is valid for $r_{ij} < L_0/2$, while the second term holds for $r_{ij} < L_0$. The correlation vanishes identically for $r_{ij} > L_0$. This analysis indicates that the density correlation observed is due to the fact that fibers span a finite spatial domain, therefore, mediating non-local interactions with a range proportional to their length.

Since the fiber number density is linearly related to the network stiffness at high densities and sufficiently large fiber stiffness (l_b) [27], a similar scaling is expected for the elastic moduli (defined over the patch of area δ^2). We study the elasticity of the network using the procedure described in the previous section. For the range of δ values considered ($\delta > \delta_0$), patches of size δ^2 are approximately elastically isotropic. Therefore, in the following we focus on the scaling properties of Young's modulus, E. The Poisson's ratio of these patches of high density results close to 0.5 [27]. Figure 3b shows the ACF of the modulus, $\mathrm{ACF}_E(r)$. A power law results for the range investigated, $\mathrm{ACF}_E(r) \sim r^{-s_E}$, with the fitted exponent approximately equal to that obtained for the density, $s_E = 0.92 \pm 0.06$. The fiber number density and the scale of observation, δ have no influence on s_E. The resulting fractal box dimension of the stiffness map is $D_E = 3 - s_E/2 = 2.54 \pm 0.03$. As for density, a cut-off is obtained at $r/L_0 \sim 0.5$.

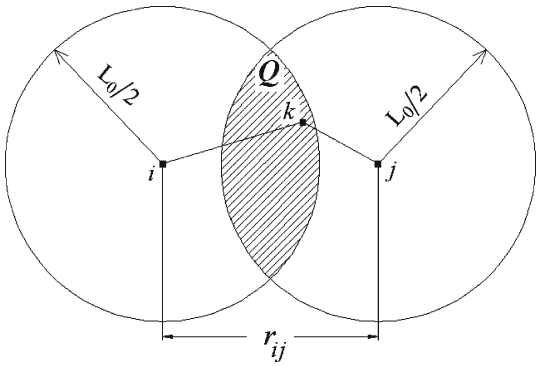

Fig. 4 Schematic plot of the domain Q over which the sum in Eq. (4) is performed. The domain Q is the intersection of two circles of radius $L_0/2$ centered at elements i and j. r_{ij} is the distance between their centers

It is also interesting to investigate the effect of the fiber bending stiffness l_b on this result. The ACF of Young's modulus E for networks with various fiber bending stiffnesses, $l_b/L_0 \in [0.0001, 0.01]$, and of same density, $l_c/L_0 = 0.009$, is shown in Fig. 5. The network elasticity is probed at $\delta/l_c = 2.27$. As the fiber bending stiffnesses decrease, the curves shift down while preserving their slope in the log–log plot. Similar results were obtained for networks with other densities and probing length scales, δ/l_c.

To understand the similarity between $\mathrm{ACF}_\rho(r)$ and $\mathrm{ACF}_E(r)$ as well as the dependence of $\mathrm{ACF}_E(r)$ on the fiber bending stiffness, let us consider the relationship between modulus and fiber density found numerically by several authors [19,27]. The modulus is linear with the density ρ above a certain threshold ρ_0. Below the threshold, the modulus dependence on density is much weaker. Let us use the approximation:

$$E(r) = \begin{cases} 0 & \rho < \rho_0 \\ \alpha(\rho - \rho_0) & \rho \geq \rho_0 \end{cases}, \tag{5}$$

Then, one can re-write the modulus ACF in terms of the density ACF:

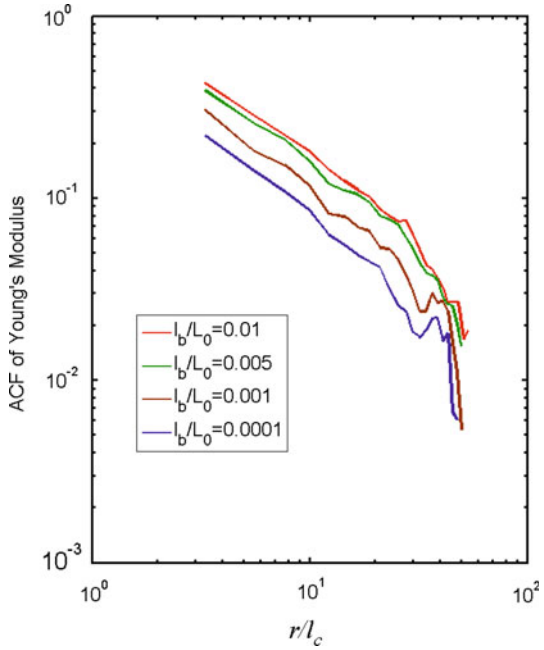

Fig. 5 Normalized auto-correlation functions (ACF) of the effective Young's modulus E distribution for networks with different fiber bending stiffness within the range $l_b/L_0 \in [10^{-4}, 10^{-2}]$ and identical mean fiber segment length $l_c/L_0 = 0.009$ (density) and probing length scale $\delta/l_c = 2.27$

$$\begin{aligned} \mathrm{ACF}_E(r) &= \langle (E - \langle E\rangle)(E - \langle E\rangle)\rangle \\ &\approx \alpha^2 \langle (\rho - \rho_0 - \langle \rho - \rho_0\rangle) \\ &\quad \times (\rho - \rho_0 - \langle \rho - \rho_0\rangle)\rangle|_{\rho>\rho_0} \end{aligned} \tag{6}$$

where only values of the density larger than ρ_0 are selected in computing the average. The constant α is eliminated after normalization with the variance. The threshold density ρ_0 is directly related to the fiber bending stiffness l_b; ρ_0 increases when l_b decreases. Expression (6) was evaluated directly from the density data for various values of the threshold. The resulting estimate of the normalized $\mathrm{ACF}_E(r)$ is a power law of exponent very close to s_E and shifts to lower values as ρ_0 increases, in a manner similar to the behavior shown in Fig. 5. Curves for the various ρ_0 remain parallel. Hence, the analysis suggests that the functional form of $\mathrm{ACF}_E(r)$ is determined by the functional form of $\mathrm{ACF}_\rho(r)$ through the piecewise linear relation (6). In the limit of very large ρ_0, the $\mathrm{ACF}_E(r)$ is expected to become a delta function; however, this limit cannot be reached in simulations since the system becomes mechanically unstable. For large values of $l_b/L_0(>10^{-1})$, the fiber bending moments become so large that local elasticity ceases to be valid on small probing length scale δ/l_c and a micro-polar formulation is required to represent the elasticity of the network.

4 Discussion and conclusions

These results show that the network deforms in a manner similar to a highly heterogeneous continuum with stochastic, long-range correlated distribution of elastic moduli. Many materials that exhibit such properties are found in nature. Examples include porous rock [28], trabecular bone [29,30], aerogels [31,32], various types of tissue [33], the skeleton of various marine diatoms [34] and materials whose microstructure is determined by diffusion-limited aggregation. The present discussion adds random semi-flexible fiber networks to this list.

In such structures, scale decoupling does not exist in the range of scales over which correlations and self-similarity are observed. This implies that multiscale modeling cannot be performed using standard information-passing techniques or the usual theoretical tools developed in homogenization theory [35]. Specialized methods such as that developed in [36,37] are required. This conclusion becomes important when addressing large problems such as that of cytoskeleton deformation. The cytoskeleton contains stiff fibers (microtubules) that span the entire cell, as well as semi-flexible F-actin fibers. The F-actin filaments with radius 4 nm and length of 2 μm have $l_b/L_0 \sim 0.002$ [19], which is within the range considered here. The present analysis suggests that the network may exhibit spatial correlations of the deformation field. Hence, "representative volume elements" can be used, and "equivalent" constitutive equations can be written only on scales larger than the upper limit of the respective scaling range. However, a complete understanding of the cytoskeleton mechanics requires more complex models that include additional physics (e.g. formation of stress fibers, myosin activity, etc.).

The fractal nature of the network geometry was observed before. Kaye [38] used the box counting method to compute the fractal dimension of networks generated in a manner similar to that considered here and obtained a scaling exponent of $D_{2D} = 1.5$. The procedure requires counting the number of squares of size δ necessary to cover the image of the network, followed by observing the scaling of this number as $\delta^{-D_{2D}}$. This method cannot be applied for $\delta > l_c$ because the entire 2D domain ends up being tiled when such large squares are used (then, the dimension D_{2D} becomes equal to that of the embedding space, $D_{2D} = 2$). This procedure produces information relevant for the "hole" size distribution of the network. The method considered here probes the fluctuations of network density and local stiffness on larger scales. The fractality of these two geometric and mechanical parameters cannot be inferred from the fractality of the geometry probed at length scales smaller than l_c.

Let us discuss the implications and transferability of these findings to other types of networks. If one considers systems composed from very long ("infinite") fibers cross-linked

at their intersection points, the present discussion holds provided the fiber length L_0 is replaced by the fiber persistence length, l_p. The persistence length is the correlation length of fiber orientation measured along given fiber. If $l_p \gg l_c$, a scaling range is expected for moduli and densities as reported in this article. This establishes a link between systems with long fibers (e.g. tissue scaffolds obtained by electrospinning) and those composed from chopped fibers.

In conclusion, it is shown that the elasticity of random semi-flexible networks is similar to that of heterogeneous media with stochastic spatially correlated moduli. Modeling the mechanics of such structures requires adopting specialized techniques designed for situations lacking scale decoupling. This becomes important when attempting to understand the complex multiscale deformation of many biological systems.

References

1. Lodish H, Berk A, Matsudaira P, Kaiser CA, Krieger M, Scott MP, Zipursky L, Darnell J (2001) Molecular cell biology. Freeman, New York
2. Stossel TP (1994) The machinery of cell crawling. Sci Am 271: 54–63
3. Chaudhuri O, Parekh SH, Fletcher DA (2007) Reversible stress softening of actin networks. Nature 445:295–298
4. Janmey PA, McCormick ME, Rammensee S, Leight JL, Georges PC, MacKintosh FC (2007) Negative normal stress in semiflexible biopolymer gels. Nat Mater 6:48–51
5. Storm C, Pastore JJ, Mackintosh FC, Lubensky TC, Janmey PA (2005) Nonlinear elasticity in biological gels. Nature 435: 191–194
6. Pullarkat PA, Fernandez PA, Ott A (2007) Rheological properties of the Eukaryotic cell cytoskeleton. Phys Rep 449:29–53
7. Cox HL (1952) The elasticity and strength of paper and other fibrous materials. Br J Appl Phys 3:72–79
8. Wu XF, Dzenis YA (2005) Elasticity of planar fiber networks. J Appl Phys 98:093501
9. Wagner B, Tharmann R, Haase I, Fischer M, Bausch AR (2006) Cytoskeletal polymer networks: the molecular structure of cross-linkers determines macroscopic properties. Proc Natl Acad Sci USA 103:13974–13978
10. Gardel ML et al (2004) Elastic behavior of cross-linked and bundled actin networks. Science 304:1301–1305
11. Astrom JA, Timonen J, Myllys M, Fellman J, LeBell J (2007) Random networks of fibres display maximal heterogeneity in the distribution of elastic energy. Eur Phys J E 22:61–66
12. Astrom JA, Makinen JP, Alava MJ, Timonen J (2005) Elasticity of Poissonian fiber networks. Phys Rev E 61:5550–5556
13. Head DA, Levine AJ, MacKintosh FC (2003) Deformation of cross-linked semiflexible polymer networks. Phys Rev Lett 91:108102
14. Heussinger C, Frey E (2006) Stiff polymers, foams, and fiber networks. Phys Rev Lett 96:017802
15. Jaeger HM, Nagel SR, Behringer RP (1996) Granular solids, liquids, and gases. Rev Mod Phys 68:1259–1273
16. Tanguy A, Wittmer JP, Leonforte F, Barrat JL (2002) Continuum limit of amorphous elastic bodies: a finite-size study of low-frequency harmonic vibrations. Phys Rev B 66:174205
17. Leonforte F, Tanguy A, Wittmer JP, Barrat JL (2004) Continuum limit of amorphous elastic bodies. II. Linear response to a point source force. Phys Rev B 70:014203
18. Hatami-Marbini H, Picu RC (2009) An eigenstrain formulation for the prediction of elastic moduli of defective fiber networks. Eur J Mech A/Solids 28:305–316
19. Wilhelm J, Frey E (2003) Elasticity of stiff polymer networks. Phys Rev Lett 91:108103
20. Liu J, Koenderink GH, Kasza KE, MacKintosh FC, Weitz DA (2007) Visualizing the strain field in semiflexible polymer networks: strain fluctuations and nonlinear rheology of F-actin gels. Phys Rev Lett 98:198304
21. Heussinger C, Schaefer B, Frey E (2007) Nonaffine rubber elasticity for stiff polymer networks. Phys Rev E 76:031906
22. Hatami-Marbini H, Picu RC (2008) Scaling of nonaffine deformation in random semiflexible fiber networks. Phys Rev E 77:062103
23. Hatami-Marbini H, Picu RC (2009) Effect of fiber orientation on the non-affine deformation of random fiber networks. Acta Mech 205:77–84
24. Kallmes O, Corte H (1960) The structure of paper. I. The statistical geometry of an ideal two dimensional fiber network. Tappi J 43:737–752
25. Hatami-Marbini H, Picu RC (2009) Two-dimensional continuum map of filamentous random networks. Bioengineering Conference, IEEE 35th Annual Northeast, Boston, pp 1–2
26. Falconer KJ (1990) Fractal geometry: mathematical foundations and applications. Wiley, New York
27. Head DA, Levine AJ, MacKintosh FC (2003) Distinct regimes of elastic response and deformation modes of cross-linked cytoskeletal and semiflexible polymer networks. Phys Rev E 68:061907
28. Kahle A, Winkler B, Radulescu A, Schreuer J (2004) Small-angle neutron scattering study of volcanic rocks. Eur J Miner 16:407–417
29. Majumdar S et al (1999) Fractal analysis of radiographs: assessment of trabecular bone structure and prediction of elastic modulus and strength. Med Phys 26:1330–1340
30. Parkinson IH, Fazzalari NL (2000) Methodological principles for fractal analysis of trabecular bone. J Microsc 198:134–142
31. Ma HS, Roberts AP, Prevost JH, Jullien R, Scherer GW (2000) Mechanical structure–property relationship of aerogels. J Non-Crystal Sol 277:127–141
32. Marliere C, Despetis F, Etienne P, Woignier T, Dieudonne P, Phalippou J (2001) Very large-scale structures in sintered silica aerogels as evidenced by atomic force microscopy and ultra-small angle X-ray scattering experiments. J Non-Crystal Sol 285:148–153
33. Maksym GN, Bates JHT (1997) A distributed nonlinear model of lung tissue elasticity. J Appl Physiol 82:32–41
34. Vrieling EG et al (2004) Ultrasmall, small, and wide angle X-ray scattering analysis of diatom biosilica: interspecific differences in fractal properties. J Mater Chem 14:1970–1975
35. Nemat-Nasser S, Hori M (1993) Micromechanics: overall properties of heterogeneous materials. North-Holland, Amsterdam
36. Soare MA, Picu RC (2008) Boundary value problems defined on stochastic self-similar multiscale geometries. Int J Num Methods Eng 74:668–696
37. Soare MA, Picu RC (2008) Spectral decomposition of random fields defined over the generalized cantor set. Chaos Solitons Fractals 37:566–573
38. Kaye BH (1989) A random walk through fractal dimensions. VCH Publishers, New York